PSFC/JA-00-36

A Study of Molybdenum Influxes and Transport in Alcator C-Mod

B. Lipschultz, D.A. Pappas, B. LaBombard, J.E. Rice,
D. Smith, S. Wukitch

November 2000

Plasma Science and Fusion Center
Massachusetts Institute of Technology
Cambridge, MA 02139 USA

This work was supported by the U.S. Department of Energy, Cooperative Grant No. DE-FC02-99ER54512.

Submitted for publication to *Nuclear Fusion.*

A STUDY OF MOLYBDENUM INFLUXES AND TRANSPORT IN ALCATOR C-MOD

B. LIPSCHULTZ, D.A. PAPPAS, B. LABOMBARD, J.E. RICE, D. SMITH, S. WUKITCH

Plasma Science and Fusion Center,

Massachusetts Institute of Technology,

Cambridge Massachusetts, 02139,

United States of America

ABSTRACT: We present a characterization of molybdenum sources, Γ_{Mo} , core Mo content, N_{Mo}, and their dependencies on Alcator C-Mod operational regimes. The primary impurity source locations are the divertor, the inner wall and the ICRF antenna limiters. Boronization is used to coat the first-wall surfaces with a thin layer of B which greatly reduces the Mo sources for a period of time, eroding away with an e-folding period of 15-50 discharges. The penetration of molybdenum into the core plasma under different conditions is analyzed using the concept of penetration factors, $PF=N_{Mo}/\Gamma_{Mo}$ (seconds). In general the inner wall Mo source is large ($\sim 10^{18}$/sec) but is found to be relatively uncorrelated with the core Mo content in diverted plasmas. The outer divertor source is of similar order to that from the inner wall and has a penetration factor in the range $10^{-5} - 2x10^{-3}$ seconds depending on density and confinement mode. The antenna limiter Mo sources are typically smaller, but with higher penetration factors of $10^{-3} - 2x10^{-2}$ seconds. The behavior of the antenna limiter sources is consistent with physical sputtering due to the influence of RF sheath rectification. Measurements of the plasma potential on field lines connected to the antenna are very high when the antennas are energized, often reaching hundreds of volts.

1. Introduction

The impurity content of the plasma core is an important factor in determining the success of any fusion experiment. As part of the effort to predict impurity levels it is important to understand the processes of impurity generation, transport in the Scrape-Off-Layer (SOL) and in the core. The effects of the type of operation (limited vs. diverted) and confinement mode (L- or H-mode) on transport are important factors as well.

High-Z materials are envisaged for use as part of the first-wall in a magnetic fusion reactor, having advantages over low-Z materials such as graphite in terms of erosion, hydrogen retention and safety concerns [1, 2]. The risk of using high-Z materials stems from the difficulty of fully-stripping them of electrons in the core plasma, leading to strong radiation losses there. If the concentration of such impurities in the core can be kept low then their advantages as a first-wall material are very compelling. Studies of high-Z sources have been performed on limiter [3-8] and divertor tokamaks[9-12]. The issue of impurity penetration to the core has often been separately addressed through examination of recycling [13-17] and nonrecycling elements [18-20, 14, 21, 15, 22, 17, 23]. The experience with high-Z materials has not been as prevalent as that with graphite, particularly in the presence of RF heating. In this paper we characterize the experience with Mo sources and their penetration to the core plasma in Alcator C-Mod, a divertor tokamak.

2. Experiment and technique

Basic characteristics of the Alcator C-Mod tokamak experiment and diagnostics are described elsewhere [24]. The data used in this study were acquired with 5.3 Tesla toroidal magnetic field at the plasma center and plasma currents in the range 0.8-1.0 MA. All discharges were diverted with a single field null at the bottom of the machine. The data in this study are primarily from ICRF-heated discharges (both L- and H-mode). The ICRF heating utilizes 2 two-strap antennas launching waves at 80 MHz [25] located at the outer midplane at 'D' and 'E' ports (antennas labeled 'D' and 'E' in Figure 1). There is also a third antenna with 4 current straps, herein referred to as the 'J' antenna. The J antenna straps can be operated in various phasing patterns corresponding to heating or current drive as well as different frequencies. For the discharges used in this study, the 'J' antenna was operated as 2 separate two-strap antennas, labeled 'J3' and 'J4' in Figure 1, at 78 MHz. All of the above antennas were primarily operated in a phasing and frequency to heat a H minority in D plasmas.

The plasma-interaction surfaces of the tokamak are all molybdenum tiles. The poloidal crossection is shown in Figure 2. Shown in the figure are the standard tokamak plasma –interaction surfaces of the lower divertor and inner wall. In addition, for protection of the antennas, there are partial poloidal limiters at the outside edge of the plasma (see Fig.1 for toroidal location) as well as tiles directly attached to the outside edge of the antennas, forming a 'picture frame'. The poloidal limiters are typically located ~1-1.5 cm radially outside the separatrix (referenced to the midplane). The antenna protection tiles and Faraday screen are located, respectively, .5 and 1.0 cm further outside the separatrix.

Boronization conditioning is performed which coats all directly accessible surfaces with an ~ 100 nm thick layer of boron. The procedure being employed utilizes Electron Cyclotron Discharge Cleaning (ECDC) to create the plasma discharge, using a helium-diborane mixture (10% B_2D_6,

90% He) as the working gas. The toroidal field, required for the ECDC resonance, is swept across the vacuum chamber. The ECDC is pulsed at a 50% duty cycle, in order to allow the diborane to spread uniformly around the chamber between pulses. The diborane is also injected into the chamber through a continuous toroidal tube with holes spaced approximately 1 cm toroidally to enhance the toroidal uniformity. The boronization process is repeated every 8-16 experimental run days due to erosion of the B layer.

The determination of Mo influx rates is based on measurements of the Mo-I line brightness at 386.4 nm (one of a three line triplet). Fiber optics are employed to relay the light collected by a number of imaging systems viewing different first-wall surfaces around the vessel to an f/4, 0.25 m visible spectrometer which simultaneously monitors 16 of those locations. The inner wall and antenna limiter surfaces are monitored with midplane radial and toroidal views respectively. The inner and outer divertor surfaces are monitored with optics at the bottom of the vessel viewing poloidally through the divertor region. The geometry of the views of different first-wall surfaces are further detailed in reference [12]. The inverse photon efficiency for the Mo-I line, also known as S/XB, is utilized to convert the Mo-I photon brightness to influx (per unit area) based on a standard formalism [5, 26]. The specific Mo-I S/XB required for this study are provided in reference [27]. The plasma density (n_e) and electron temperature (T_e) in the SOL and at the divertor plate needed for determination of inverse photon efficiencies are measured by Langmuir probes [28]. n_e and T_e measurements at the divertor plates are routinely made with an array of spatially-fixed probes. Measurements in the SOL are made more infrequently with a spatially-scanning Langmuir probe, and as such, we assume constant values of n_e (1.0×10^{19} m^{-3}) and T_e (25 eV) at the inner wall and antenna protection tile Mo source locations for the determination of the local S/XB. Note that the Mo-I S/XB varies very slowly with density and only a factor of 2 in changing T_e from 10 to 25 eV. The total impurity source, Γ_{Mo}, assigned to a first-wall component, is taken to be the local impurity influx (#/sec/m^2) multiplied by the plasma-facing area of that component.

The core Mo content is determined from the brightness of a Mo^{33+} line at 0.374 nm using an x-ray crystal spectrograph [29]. Core n_e and T_e profiles are used to model the brightness of the spectrometer's chordal view through the plasma. The Mo^{33+} density is then determined by matching the measured and modeled Mo^{33+} brightnesses. The total Mo density (sum over all charge states) has been found to be fairly flat in radial profile. Thus one only needs the plasma volume (~1.0 m^3) to determine the total core Mo content, N_{Mo}. More details of this method are found elsewhere [29].

The concept of penetration factor, PF, has been defined previously [20, 17] as the ratio of a given core impurity content (total), N_Z, to its corresponding source, Γ_Z at the first wall:

$$PF=N_Z/\Gamma_Z. \quad (1)$$

The relationship between the probability that an impurity neutral will enter the core, η_Z, and PF is defined as [16]:

$$\eta_Z = PF/\tau_Z, \quad (2)$$

where τ_Z is the core impurity confinement time. In general we will be referring to penetration factors in this paper.

The energy of ions striking a first-wall surface is, to a large degree, determined by the plasma potential, V_P. Thus this parameter is important for estimating the Mo physical sputtering rate. We normally calculate the plasma potential based on the Langmuir probe measurement of floating potential, V_F, the local plasma temperature and basic sheath theory:

$$V_P \sim V_F + 3xT_e. \quad (3)$$

As part of these experiments we made an effort to more directly determine the plasma potential using an emissive probe technique [30-33]. Thoriated tungsten filaments were located on 2 sides of a poloidal limiter on field lines that directly connect to two of the antennas labeled 'D' and 'J4' in Figure 1. High frequency AC current (60 kHz) was employed to heat the .125 mm dia. filaments in the presence of the toroidal magnetic field without breaking. At such elevated temperatures (~1800 ^oC) the filament is in a regime where the emitted electron current was greater than the free-streaming electron flux. The floating potential of such a heated filament is thus a measure of the plasma potential to within ~ T_e [33].

3. Source characterization

3.1 general characteristics

The most important Mo sources are the outer divertor, sections of the inner wall near the midplane and, for ICRF-heated discharges, the antenna protection limiters. The remainder of the inner wall, the inner divertor and the outer poloidal limiters are infrequent contributors as Mo sources. This is likely due to those areas receiving low local ion fluxes and/or electron temperature are low. In the case of the inner divertor this is most often the result of plasma detachment there. Figure 3 illustrates the relative strengths of the relevant sources and the variations that can occur during a single shot. The plasma switches from being limited on the inner wall to diverted near the beginning (~0.25 seconds) and end of the shot as indicated by the trace detailing the separatrix to inner-wall gap (3b). The ICRF power is on from .5 to 1.2 seconds (3b). The core confinement switches from L- to H-mode at ~ 0.92 seconds, as evidenced by the rise in core density (3a). Note that this particular H-mode is ELM-free, which not only leads to increased energy confinement, but also leads to impurity accumulation.

Of primary interest is the core Mo density shown in Fig. 3e. It is highest during the period when the plasma is limited on the inner wall and drops as the plasma becomes diverted. The core Mo content increases again when RF power is injected, further increasing when the plasma energy

confinement changes from L- to H-mode. The core Mo content would rise during H-mode even if the Mo source rate stays constant, given that the impurity confinement increases [34]. The inner wall source (3d) is largest during the period when the plasma is limited and then steadily decreases throughout most of the shot, dropping dramatically during the ELM-free phase. The lack of correlation between wall source and core content for diverted plasmas as seen in this figure is typical, even though the wall source is of similar order or larger than other sources.

The core Mo content is more correlated to the outer divertor source (3d). Again referring to Fig. 3, the divertor Mo source increases as the plasma becomes diverted, with a second increase following injection of RF power. Interestingly, the outer divertor source also decreases during the ELM-free H-mode period. ELM-free H-modes in Alcator C-Mod are typically characterized by a large increase in core impurity radiation due to increases in core density and impurity confinement time. The drop in Mo source rate at the outer divertor and inner wall is correlated with the resultant decrease in power flow across the separatrix, and to the divertor.

The clearest correlation between a Mo source and the core Mo content is that of the antenna (3c). It rises when the RF power is injected, increases proportionally to the RF power and then returns to insignificant levels after the RF is off. Unlike the wall and divertor Mo sources, the antenna protection tile source rate is not affected by the change in confinement with the corresponding drop in power flowing into the SOL. The magnitude of the antenna source is less than that from the inner wall and divertor.

To add further evidence of the lack of correlation between the inner wall source and the core Mo content we have examined the effect of varying the inner gap. In Figure 4 we plot the inner wall source and the core Mo density for several different gaps. These data points are all for constant plasma density, 0.6-1MW of ICRF power and L-mode confinement. The inner wall source decreases as the gap increases. The core Mo content data is scattered but evidence no trend.

3.2 Scaling of Mo sources

To explore the correlation between the antenna source and core Mo content further we refer to Figure 5. These data are from a series of discharges where the density was held constant at $\bar{n}_e = 2.0 \times 10^{20}$ m^{-3}. To eliminate the effect of confinement changes the RF power was held to levels under 1 MW, below the H-mode power threshold for this run day. The wall source was essentially constant, again showing lack of correlation with the core Mo content. The core Mo content and the antenna Mo source rate rise linearly with RF power, increasing by factors of 6-8. The outer divertor Mo source initially increases more slowly as a function of RF power, increasing more rapidly at higher RF powers.

The general ordering of the magnitudes of different impurity sources does vary as plasma conditions vary. For example the plasma density appears to be an important parameter, as seen in

Figure 6a-c. Although there is significant scatter in the data, due primarily to variations in RF power, there is a trend for all sources to decrease with increasing density. The fractional decrease is largest for the divertor which, although the largest at low densities, drops to levels approaching the other source rates for $\bar{n}_e$ ~$1.5x10^{20}$ m^{-3}. At densities above $2.0x10^{20}$ m^{-3} the plasmas are in H-mode. These data are quite scattered, with some tendency towards increased source levels compared to L-mode.

4. Boronization

All of the discharge data shown in Figure 6 are from plasma discharges which were run several weeks (~100-200 discharges) after a vessel boronization. The Mo source levels and core Mo content fall to very low levels immediately following a boronization and then slowly recover afterwards. This is illustrated in Figures 7-8. The first of these figures shows the effects of boronization for the *limiter* phase of discharges. Both the Mo source rate and core content drop by a factor of ~50 following boronization, The recovery back to pre-boronization levels occurs with an e-folding of ~50 discharges. Note that these discharges were only limited for a short phase during plasma current rise (~.3 seconds) and current rampdown.

The effect of boronization on Mo source levels and core content during *diverted* periods of the same discharges is shown in Figure 8. ICRF is utilized ('E' antenna only) for heating and the plasma is in H-mode. There are similarities and differences to figure 7 above. The inner wall and outer divertor sources (8a) also drop after boronization, but by lesser amounts (x10) than in limited discharges. The effect of boronization is much shorter-lived for the outer divertor, of order 15-20 discharges. This indicates that the removal of B from those surfaces, presumably by sputtering, is much faster. This is not surprising, given the high particle fluxes in this region which lead to the highest Mo source rates in the diverted phase of discharges.

The D antenna (Figure 8b) is not being used during these discharges. The Mo source rate from this location in the shadow of the poloidal limiters is affected little by the boronization and afterwards. This is not surprising given the low power and particle fluxes in this region. The core radiated power (Figure 8d) also shows minimal change after boronization. Since the Mo core content (8c) and radiation have essentially been reduced to below the measurement limit after boronization, we speculate that the Mo radiation in the pre-boronization discharges, although significant, did not dominate the core radiation. We do not have direct measurements of the core content of B and other low-Z impurities at this time. Based on the B content at the edge (~1% of n_e), and assuming that the core levels are similar, we believe that B dominates the core Z_{eff} in the majority of discharges. It is likely that B also dominates core radiation losses for at least the post-boroniztion discharges.

Both the E antenna source (8c) and the core Mo content also drop less after boronization than in the limited phase of these discharges, but correlate well as expected from the data shown in figures 3 and 5. Again, we find that the best source correlation with the core Mo content is the E antenna source during ICRF-heated discharges.

5. Penetration factors

It is unfortunate that we cannot easily isolate one Mo source from another with respect to their importance in determining the core Mo content. We can perhaps shed some light on the relative contribution to the core N_{Mo} by different sources through examination of the penetration factor for the outer divertor (PF_{OD}) and antenna protection tiles (PF_{ANT}) as seen in Figures 9a-b (open symbols). Note that we use the *total* core Mo content in calculating each PF; the PF shown is thus an upper bound. In general, PF_{ANT} is considerably higher than PF_{OD}, except for densities above $1.5x10^{20}$ m^{-3}. In addition the lowest PFs for antenna and outer divertor sources *are almost 2 orders of magnitude apart.* Wall penetration data is not included here because of the lack of correlation with the core Mo content, and thus the inability to estimate a PF.

The shots included in this database have been examined for variations in source rates and core content, such as that shown in Figure 3, in order to determine which data points are from discharges where N_{Mo} appears to be dominated by either the antenna or outer-divertor Mo sources. Based on that subjective analysis we find that the antenna source 'dominates' over that of the outer divertor for cases where $\Gamma_{ANT}/\Gamma_{OD} > 0.1$. The filled datapoints of Figures 9 represent such cases of divertor (9a), and antenna protection tile (9b) source dominance.

6. Discussion

6.1 Penetration of Mo into the core plasma

The outer divertor source appears to dominate the core Mo content during diverted ohmic discharges. With the addition of ICRF heating the antenna protection tile sources become important. The higher penetration factor for impurity sources at the outer midplane often leads to the antenna sources being the primary contributor to core Mo content. The fact that the antenna source dominates over the outer divertor source for $\Gamma_{ANT}/\Gamma_{OD} > 0.1$ is simply a reflection of the relative effect on the core Mo content through the relevant penetration factor:

$$N_{Mo} \text{ (due to antenna source)} = PF_{ANT} \, x\Gamma_{ANT}. \quad (4)$$

This leads to the equivalent description of when the antenna source dominates over that from the outer divertor:

$$\Gamma_{ANT}/\Gamma_{OD} > PF_{OD}/\, PF_{ANT} \, . \quad (5)$$

The penetration factors obtained where one source or the other is 'dominant' are similar to that obtained in previous C-Mod studies utilizing injection of N_2 and CH_4 from different poloidal

locations [23]. That study consisted of a series of discharges with $\bar{n}_e \sim 1.3 - 1.8 \times 10^{20} m^{-3}$, where N_2 and CH_4 gas were injected from the inner wall, divertor and outer wall. The resultant *divertor* PFs for injection of carbon and nitrogen are summarized from reference [23] in Fig. 9a as dashed circles and ellipses to cover the range of data presented in that reference. These divertor N_2 and CH_4 injection data are similar to that obtained for inner wall gas injection, and somewhat higher than the divertor Mo PFs obtained in the present study. The PF values for injection of gas from the outer midplane (Fig. 9b) are higher, $10^{-3} - 2x10^{-2}$ sec, similar to that obtained for Mo sources at that location. The trend of decreasing PF with increasing density is true both for gases and Mo.

The ionization mean free paths in the far SOL for Mo and N are ~2 and 6 mm respectively, calculated using a local parameters of $n_e = 1.0 \times 10^{19}$ m^{-3} and $T_e = 10$ eV, and an energy of injected N and sputtered Mo neutrals of 0.03 eV and 20 eV respectively. We use a high energy for the sputtered Mo to take into account the effect of the large number of sputtered neutrals that are ejected at energies significantly above the peak in the Thompson distribution (one half the surface binding potential of 7 eV for Mo) [35]. The mean free path scales as the square root of the sputtered neutral energy. In any case, it would seem likely that both the injected N and sputtered Mo are ionized far from the separatrix. In that case transport, which we don't expect to be very different for these elements, would determine the impurity content in the core.

There are further similarities between the Mo, N and C penetration factors. As mentioned above, the inner wall penetration factors for N and C are much lower than from the outer midplane. This inequality in penetration factors between inner and outer midplane appears to hold for Mo as well: We find that the inner wall source does not correlate with core Mo content when the plasma is diverted. Since the Mo source levels are always larger for the inner wall than for the antenna, any estimate of the inner wall Mo penetration factors must be lower than for the antenna. Furthermore, penetration factors for the inner wall source for *limited* discharges can be calculated based on boronization data for the limiter phase of discharges (Figure 7) and are similar to that of the outer divertor. It would seem likely that as the inner gap is increased (switching to diverted plasma) that the penetration factor would be lowered further.

One might expect the inner and outer midplane to be equivalent in terms of impurity penetration into the core. The question of why such low penetration factors are found for inner wall sources in C-Mod was addressed for non-recycling gases by McCracken [23]. The modeling therein identified the most plausible basis for the in-out asymmetry as being due to a combination of enhanced recycling at the inner wall and short field line lengths near the surface. The former leads to high Mach number plasma flow (M~0.3 measured towards the divertor) and thus frictional forces on the impurities. Such entrainment of impurities, when added to a short connection length to the wall in that region, results in short parallel travel times back to the wall for impurities

'launched' near the inner wall. At the outer midplane the field line lengths are considerable longer (~x10) and the measured Mach numbers are lower (~.1). In addition, the flow is away from the divertor in some sections of the outer midplane SOL [36]. Assuming that perpendicular diffusion is the same at the inner and outer midplane then the ratio of parallel to perpendicular travel times will be much lower at the inner midplane leading to better screening there. If, in addition, perpendicular transport is enhanced at the outer, compared to the inner, midplane, then the asymmetry in penetration factors between the two locations would be further increased.

As mentioned in the introduction, one can extract information about impurity screening from PF using knowledge of the core impurity confinement time, τ_Z (Eq. 2). Typical values of τ_Z in C-Mod are ~ 20 ms and 20-200 ms for L and EDA H-modes, respectively. The resultant η_{ANT} is 5-100% for L-mode and 2-10% for EDA H-modes. The outer divertor η_{OD} are 0.1–1.5% in L-mode and 0.1-1.0% in EDA H-modes. The screening of antenna-generated Mo is of similar magnitude to that obtained from laser-blowoff of Sc at the midplane [15]. As seen in previous work [20] the divertor impurity source is much better screened than that from the midplane, although in this study the ratio $\eta_{Midplane}/\eta_{Divertor}$ (corresponding to $\eta_{ANT}/\eta_{Divertor}$ for the Mo data) tends to be slightly larger.

6.2 Antenna protection tile source rates

The question arises as to why the antenna protection tiles are such a significant source of impurities. The poloidal limiters, mentioned earlier, are 5 mm closer to the separatrix and yet are considerably smaller sources of Mo (typically below the spectrometer noise level). When the SOL heat flux is reduced during ELM-free H-modes the outer divertor and inner wall sources drop, but the antenna source, which is at larger minor radii, does not. *In fact it stays proportional to the ICRF power*. The plasma in the region of the antenna has much lower densities than the outer divertor ($\leq 1 \times 10^{19} m^{-3}$ vs 1-10 x 10^{20} m^{-3}), similar plasma temperatures (5-10 eV) and much smaller Mo emission area. Thus, one would expect the antenna source to be negligible compared to the divertor. This hypothesis is supported by the behavior of the D antenna Mo source after boronization: In the absence of the antenna being energized, the erosion of Mo from that antenna is minimal.

All these differences point towards the possibility that additional mechanisms are enhancing Mo physical sputtering at the antenna tiles, most likely due to the presence of ICRF. As a working hypothesis, we point towards previous work with ICRF where sheath-rectification, leading to enhanced plasma potentials and sputtering, was identified as the cause of impurity generation [37-42]. A simple explanation of this effect is given in [42]. In short the model is that an electrical circuit is formed by parts of the antenna and field lines connecting them (and possibly the wall). The flux changes in this loop at RF frequencies lead to voltages induced on field lines at RF

frequencies. The electrons are much more mobile. In order to keep the time-averaged current to zero the plasma potential rises to inhibit electron flow. This induced plasma potential is essentially DC, leading to the term sheath-rectification.

We first examine this effect in C-Mod by measuring the floating potential, V_F, and T_e profiles with a Langmuir probe. The plasma potential is calculated based on Eq. 3 and shown in Figure 10. The addition of RF with standard heating phasing (0: π) raises V_P by 10's of volts only on field lines connected to the antenna protection tiles. The potential is increased further on those field lines when the antenna is operated with phasing poorly optimized for heating the core plasma (0: 0.3π). Such an increase in the plasma potential would significantly increase the ion sputtering yield of Mo. The probe utilized for the measurements of Fig. 10 samples plasma on field lines directly connected to the antenna. A second probe, which samples SOL plasma on field lines which are not connected to the antenna, measures no enhancement of the plasmas potential when the RF is on.

The determination of plasma potential from Langmuir probe measurements is plagued by concerns regarding the validity of the data. For example, could sheath rectification be affecting the Langmuir I-V trace? This would cause the T_e measurement to be inaccurate. Is the plasma potential dependence on floating potential and T_e (Eq. 3) valid for such regimes?

A more direct measurement of the plasma potential is made using the emissive probes described in section 2. Figure 11 contains data from two identical discharges. For one discharge, the emissve probes were heated, thus measuring plasma potential (circles). In the second discharge they were not heated, leading to a measurement of the floating potential (square symbols). The RF power was increased stepwise for the two antennas sequentially (Fig. 11a). We see that the potentials measured with the probes in emission are much higher than when not heated, thus a good indication that the probe measurement is approaching the plasma potential. We also note that the plasma potential is only high when the antenna connected by a field line to the specific probe is energized; D antenna with emissive probe 2, J4 antenna with emissive probe 1. The potentials correlate somewhat with RF power, and thus RF electromagnetic fields. The highest potentials, up to 400 volts, are measured at the highest powers. However, the measured plasma potentials do not increase proportionally to each step in RF power. In fact, even for the case of almost constant RF power, the variation in measured plasma potential on field lines connected to the antenna can be large. This is demonstrated in Figure 12.

The measurements of figures 10-12 are consistent with sheath rectification occurring on field lines connecting parts of the antenna to other surfaces in the vessel. We cannot rule out the possibility that such potentials are also being induced on field lines connecting antenna protection tiles on one edge of the antenna to tiles on the opposite edge, across the face of the antenna. However, if such induced potentials exist it is likely that they are lower than outside the antenna.

This is because when the antenna is operated as a dipole (the case here) there is an electric field null in front of the antenna.

The measured plasma potentials are large enough to be consistent with a strong Mo source from a small emitting area like the antenna protection tiles. We have previously modelled the Mo sputtering process in Alcator C-Mod and determined that the boron fraction, n_B/n_e, is of order 1% and that the dominant (sputtering) ionization state of B is B^{+3} [12]. Nachtrieb [43] has verified this model with experimental measurements; the density of B^{+3}, B^{+2}, and B^{+1} have similar levels in the far SOL, each close to 2% of the local electron density. Assuming V_{Plasma}=200 V (Mo sputtering yield ~ 0.12 Mo atoms per incident B^{+3} ion), an affected area of 5 cm^2, and the plasma parameters at the antenna mentioned above, the total Mo source rate would be $2x10^{17}/m^2/sec$, comparable to the measured antenna sources. An affected area of ~ 5 cm^2 is consistent with video camera images of the antennas which shows unfiltered visible light at localized regions along the antenna protection tiles.

The high energies of impacting ions gained from enhanced sheath potentials could potentially affect the antenna limiter Mo penetration factors. As mentioned earlier, boron ions with high incident energies (e.g. ~ 100 eV) lead to a significant population of sputtered Mo with high energies compared to the peak in the Thompson distribution. This effect would be further enhanced by the occurence of sheath rectification. For example, T_e in the region of the antenna SOL might be 5-10 eV in the absence of RF, corresponding to sheath potentials in the range 30-60 eV. The non-RF plasma potentials would then be a factor of 5-10 lower than measured during RF, leading to large enhancements in sputtered Mo energies, and possibly enhancing the Mo penetration factor for that source location.

7. Summary

The most important Mo source locations which affect diverted discharges are the outer divertor, the inner wall and the ICRF antenna protection limiters. Depending on plasma density, level of injected RF power and the confinement mode, different source locations appear to dominate the core Mo content. In general the inner wall Mo source is large ($\sim 10^{18}$/sec) but is found to be relatively uncorrelated with the core content of Mo in diverted plasmas. The outer divertor source is of similar order to that from the inner wall and has a penetration factor in the range 10^{-5} – $2x10^{-3}$ seconds, highest for low densities and H-modes. The antenna protection tile Mo sources are typically smaller, but with higher penetration factors, 10^{-3} – $2x10^{-2}$ seconds, having a dependence on density and confinement mode similar to the divertor sources. The penetration factors from the different locations are consistent with that obtained previously with non-recycling gases; divertor sources are better screened from the core than that from the outer midplane. We speculate that the lower PFs from the inner wall are attributable to the short connection lengths and

high background plasma flow in that region which would reduce the travel time to the wall. Screening efficiencies for the different locations are estimated based on core impurity confinements times. They scale the same, in terms of location and density, as the penetration factors.

The outer divertor source appears to dominate the core Mo content during diverted ohmic discharges. With the addition of ICRF heating the antenna protection tile sources, even though generally smaller than that of the outer divertor, become important. Such lower magnitude impurity sources, originating from the outer midplane, can be the dominant contributor to the core Mo content when the penetration factor is larger there (eq. 5).

Boronization leads to a dramatic reduction in both the Mo sources and core Mo content. The e-folding time for return to pre-boronization levels varies between 15-50 1.5 second discharges, depending on the first-wall location. The B layer at the outer divertor is eroded most rapidly. We believe this is due to the high power and particle fluxes incident there.

The behavior and magnitude of the antenna limiter sources is consistent with physical sputtering due to the influence of RF sheath rectification. Measurements of the plasma potential profile and its dependence on RF power show an enhancement of the potential on field lines connected to the antenna.

Acknowledgments

The authors wish to thank the entire Alcator group for assistance in acquiring this data. The authors gratefully acknowledge helpful discussions with G.M. McCracken, C.S. Pitcher and J.L. Terry. This work was supported by the U.S. Dept. Of Energy under grant DE-FC02-99ER54512.

References

[1] Wong, C.P.C., et al., Fusion Engineering & Design **38** (1997) 1.

[2] Stambaugh, R., et al., Nucl. Fusion **39** (1999) 2391.

[3] Lipschultz, B., LaBombard, B., Marmar, E.S., Pickrell, M.M., and Rice, J.E., J. Nucl. Mater. **128-129** (1984) 555.

[4] Rice, J.E., Marmar, E.S., Lipschultz, B., and Terry, J.L., Nucl. Fusion **24** (1984) 329.

[5] Behringer, K., Summers, H.P., Denne, B., Forrest, M., and Stamp, M., Plasma Phys. Control. Fusion **31** (1989) 2059.

[6] Philipps, V., et al., Nucl. Fusion **34** (1994) 1417.

[7] Neu, R., et al., J. Nucl. Mater. **241-243** (1997) 678.

[8] Unterberg, B., et al., J. Nucl. Mater. **241-243** (1997) 793.

[9] Field, A.R., et al., J. Nucl. Mater. **220-222** (1995) 553.

[10] Krieger, K., et al., J. Nucl. Mater. **241-243** (1997) 684.

[11] Thoma, A., et al., Plasma Phys. Control. Fusion **39** (1997) 1487.

[12] Pappas, D.A., Lipschultz, B., LaBombard, B., May, M.J., and Pitcher, C.S., J. Nucl. Mater. **266-269** (1999) 635.
[13] Belanger, C., et al., Nucl. Fusion **31** (1991) 561.
[14] McCracken, G.M., et al., Nucl. Fusion **33** (1993) 1409.
[15] Graf, M.A., et al., Rev. Sci. Instrum. **66** (1995) 636.
[16] Granetz, R.S., et al., J. Nucl. Mater. **241-243** (1997) 788.
[17] McCracken, G.M., et al., J. Nucl. Mater. **241-243** (1997) 777.
[18] Fussmann, G., et al., J. Nucl. Mater. **145-147** (1987) 96.
[19] Roth, J. and Janeschitz, G., Nucl. Fusion **29** (1989) 915.
[20] Janeschitz, G., et al., J. Nucl. Mater. **196-198** (1992) 380.
[21] Whyte, D., et al., Nucl. Fusion **34** (1994) 203.
[22] Philipps, V., et al., in EPS conference (Proc. of the 22nd European Phys. Soc. Conf. on Contr. Fusion and Plasma Phys., Bournemouth, U.K., 1995), EPS conference series, Vol. 19C, (1995) II/321.
[23] McCracken, G.M., et al., Phys. Plasmas **4** (1997) 1681.
[24] Hutchinson, I.H., et al., Phys. Plasmas **1** (1994) 1511.
[25] Golovato, S.N., et al., in Radio Fequency Power in Plasmas (Proc. of the 11th Topical Conf., Palm Springs, Ca. U.S.A., 1996), Radio Fequency Power in Plasmas series, Vol. 355, AIP New York (1996) 23.
[26] Fussmann, G., Hofmann, J.V., Janeschitz, G., and Yang, H.R., Nucl. Fusion **30** (1990) 2319.
[27] Badnell, N.R., Gorczyca, T.W., Pindzola, M.S., and Summers, H.P., J. Phys. B: Atom. Mol. & Opt. Phys. **29** (1996) 3683.
[28] LaBombard, B., et al., Phys. Plasmas **2** (1995) 2242.
[29] Rice, J.E., et al., J. Phys. B: Atom. Mol. & Opt. Phys. **29** (1996) 2191.
[30] Kemp, R.F. and Sellen, J.M., Rev. Sci. Instrum. **37** (1966) 455.
[31] Smith, J.R., Hershkowitz, N., and Coakley, P., Rev. Sci. Instrum. **50** (1979) 210.
[32] Wang, E.Y., Hershkowitz, N., Intrator, T., and Forest, C., Rev. Sci. Instrum. **57** (1986) 2425.
[33] Wang, E.Y., et al., J. Appl. Phys. **61** (1987) 4786.
[34] Rice, J.E., et al., Phys. Plasmas **4** (1997) 1605.
[35] Langley, R.A., et al., in Nucl. Fusion (IAEA, Vienna (1984), Vienna, 1984), Vol. Special Issue, IAEA.
[36] LaBombard, B., et al., J. Nucl. Mater. **241-243** (1997) 149.
[37] Perkins, F.W., Nucl. Fusion **29** (1989) 583.
[38] Myra, J.R., D'Ippolito, D.A., and Gerver, M.J., Nucl. Fusion **30** (1990) 845.

[39] Majeski, R., et al., in Radio Frequncy Power in Plasmas (Proc. of the 9th Topical Conf., Charleston, S.C. USA, 1991), Radio Frequncy Power in Plasmas series, Vol. 244, AIP New York (1991) 322.

[40] Bures, M., et al., Nucl. Fusion **32** (1992) 1139.

[41] Hershkowitz, N., et al., 'Reduction in SOL V_plasma increases and impurity generation caused by RF near omega_ci by the use of insulating Faraday shield limiters in the Phaedrus-T tokamak and by elimination of Faraday shields.', U. of Wisc. report# PLR-92-14, 1992, Reduction in SOL V_plasma increases and impurity generation caused by RF near omega_ci by the use of insulating Faraday shield limiters in the Phaedrus-T tokamak and by elimination of Faraday shields.

[42] Majeski, R., et al., Fusion Engineering & Design **24** (1994) 1.

[43] Nachtrieb, R.T., LaBombard, B., and Thomas, E., 'Omegatron ion mass spectrometer for the Alcator C-Mod tokamak.', M.I.T. report# PSFC/JA-00-3, 2000, to be published in Rev. Sci. Instrum.

Figure Captions

Figure 1: Plan view of the C-Mod vessel identifying the different antennas and their location relative to each other and the emissive probes.

Figure 2: Poloidal crossection of the Alcator C-Mod vessel. The location of the significant Mo source locations are the inner wall, outer divertor, and antenna protection tiles.

Figure 3: Discharge parameters: a) line-averaged density, $\bar{n}_e$; b) separatrix to inner-wall gap and ICRF power (dashed line); c) Mo source rate from the antenna protection tiles; d) Mo source rate from outer divertor and inner wall (dashed line); and (e) total core molybdenum content, N_{Mo}. H-mode starts and ends at ~.93 and 1.23 seconds respectively.

Figure 4: Variation of the inner wall Mo source and core Mo content with inner wall gap.

Figure 5: Variation of Mo sources with ICRF power for a series of L-mode discharges at $\bar{n}_e$ ~2.0×10^{20} m^{-3}.

Figure 6: Variation of Mo sources (a-c) with $\bar{n}_e$. Data are from discharges several weeks after a boronization. H-mode cases indicated by circles, L-mode by squares.

Figure 7: Effect of boronization for the portion of discharges limited on the inner wall. Shown are the inner wall Mo source and the core Mo density.

Figure 8: Effect of boronization for diverted portion of discharges. Shown are a) the Mo source rate at the outer divertor and inner wall, b) Mo source rate from the 'D' antenna protection tiles, c) Mo source rate at the 'E' antenna protection tiles with the core Mo content, and d) the core radiated power.

Figure 9: Mo penetration factors for the outer divertor (a) and antenna protection tiles (b) for the same discharges as Figure 6. Cases where a particular source (e.g. antenna protection tiles) is dominant are shaded. Penetration factors for CH_4 and N_2 injection [23] are also shown as dashed circles and ellipses to represent the multiple data points in the original paper figure.

Figure 10: Plasma potential in the SOL inferred from Langmuir probe measurements for cases with and without ICRF.

Figure 11: Emissive probe measurements of the plasma potential from probes 1 (b) and 2 (c) during two identical discharges where the antenna power (a) on 2 different antennas was increased in a stepwise fashion. In one discharge (square symbols) the probes were not heated, thus just measuring the floating potential. In the second discharge the probe were emitting (circle symbols). The antenna and emissive probe locations are shown in Figure 2.

Figure 12: Example of variation of plasma potential in a single discharge. Here only the J4 antenna was energized (a). Probe 1 (b) was heated for emission and thus measuring the plasma potential. Probe 1 is connected along a field line to the J4 antenna.

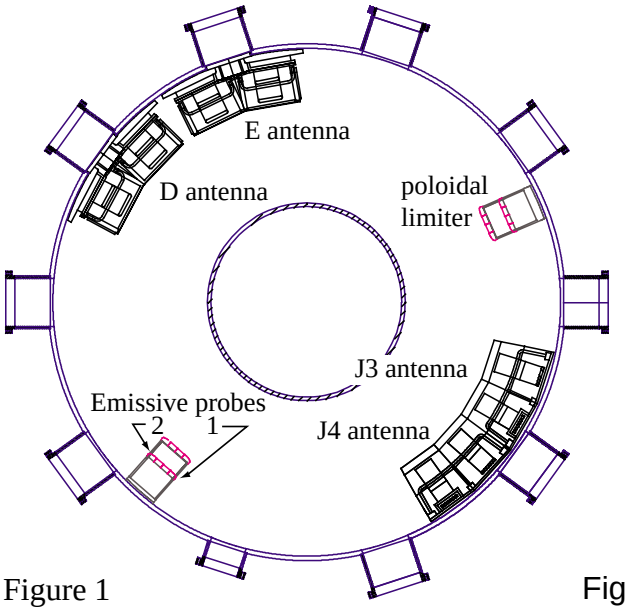

Figure 1

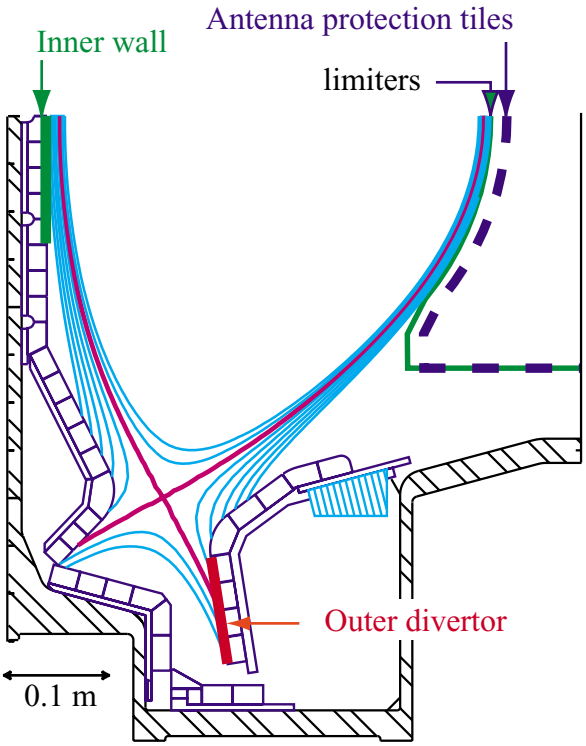

Figure 2

Figure 3

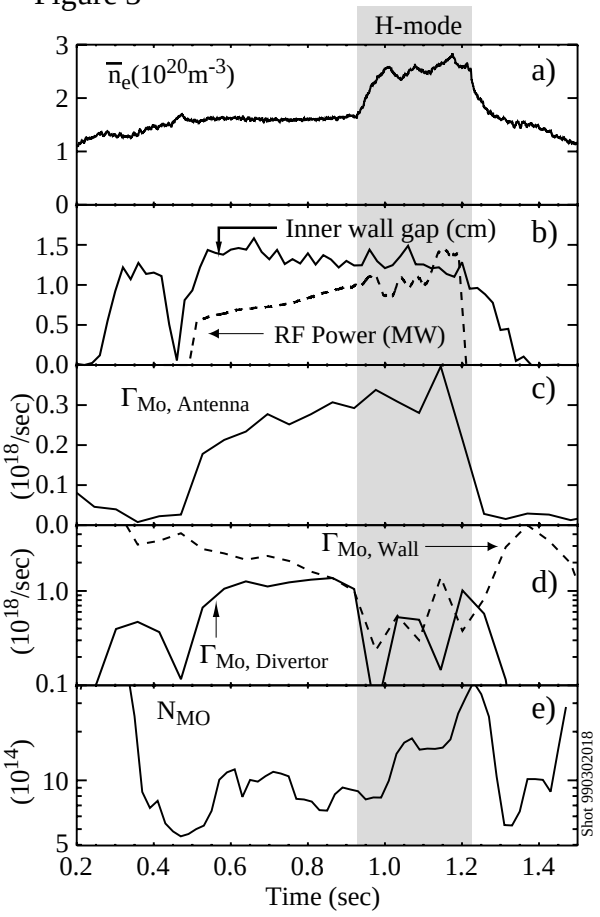

Figure 4

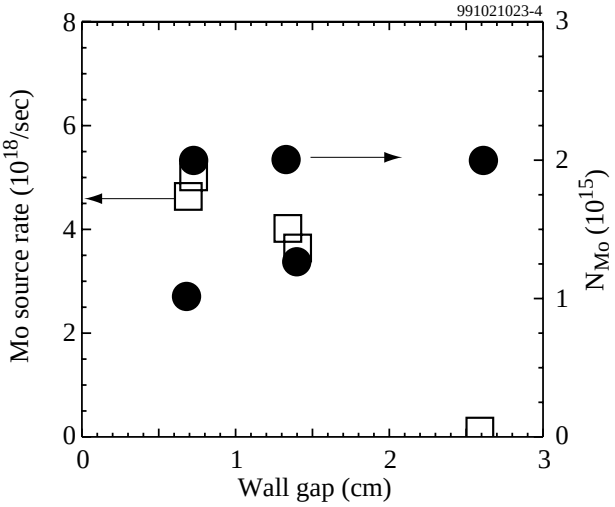

Figure 5

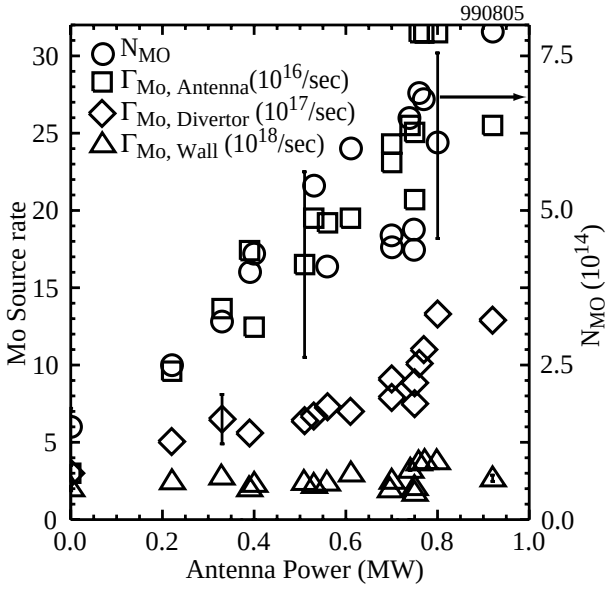

Figure 6

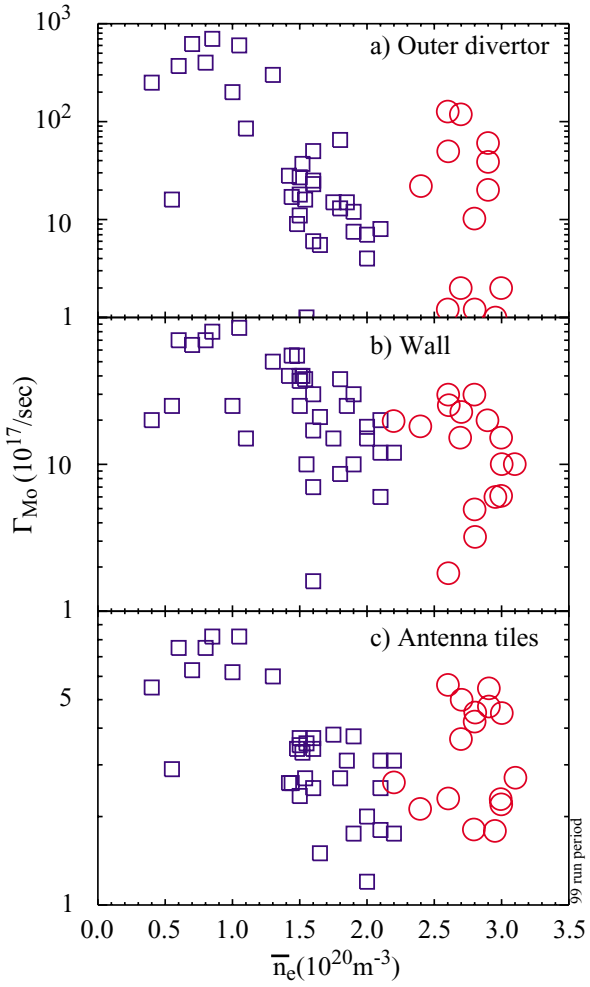

Figure 7

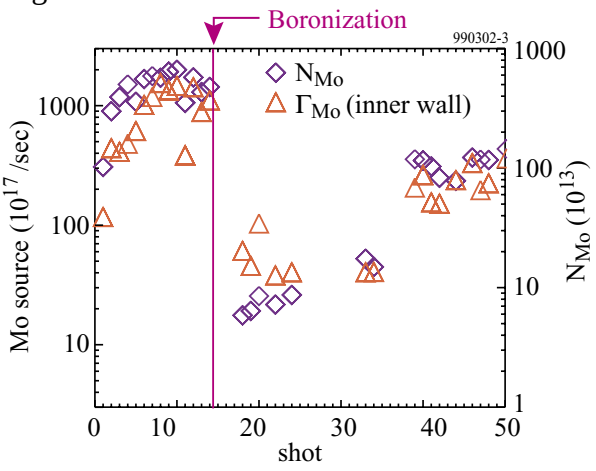

Figure 8

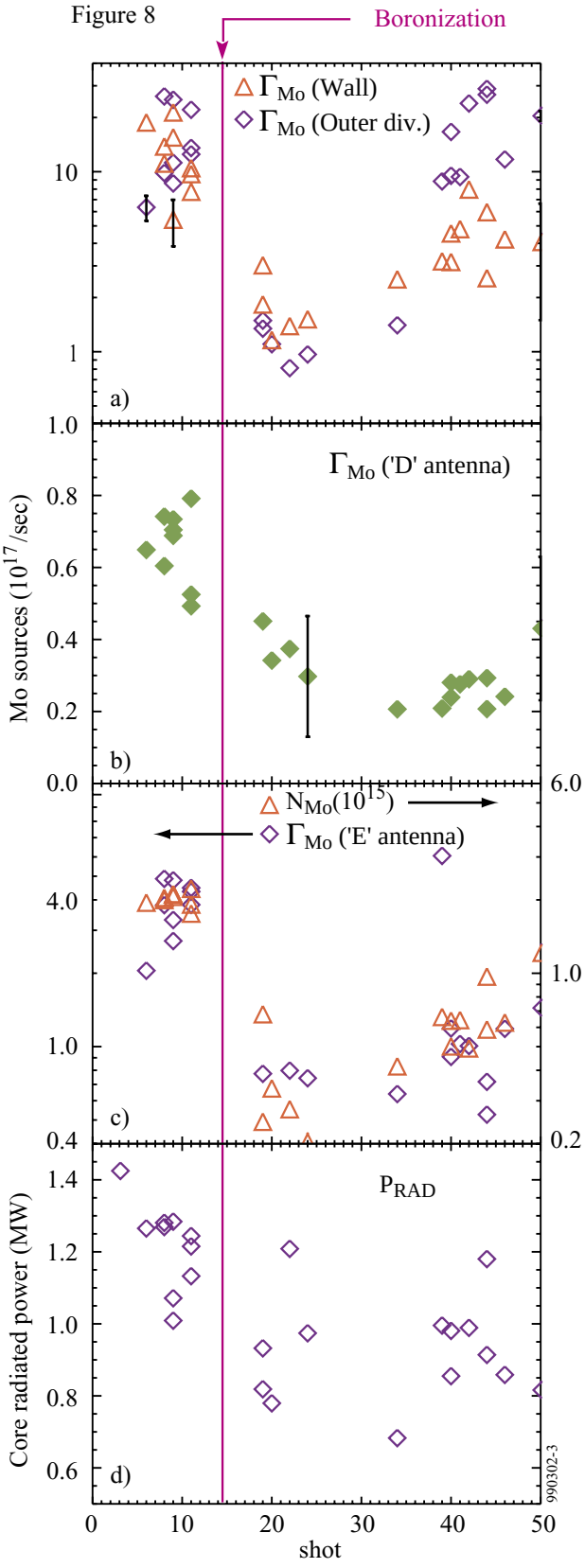

Figure 9

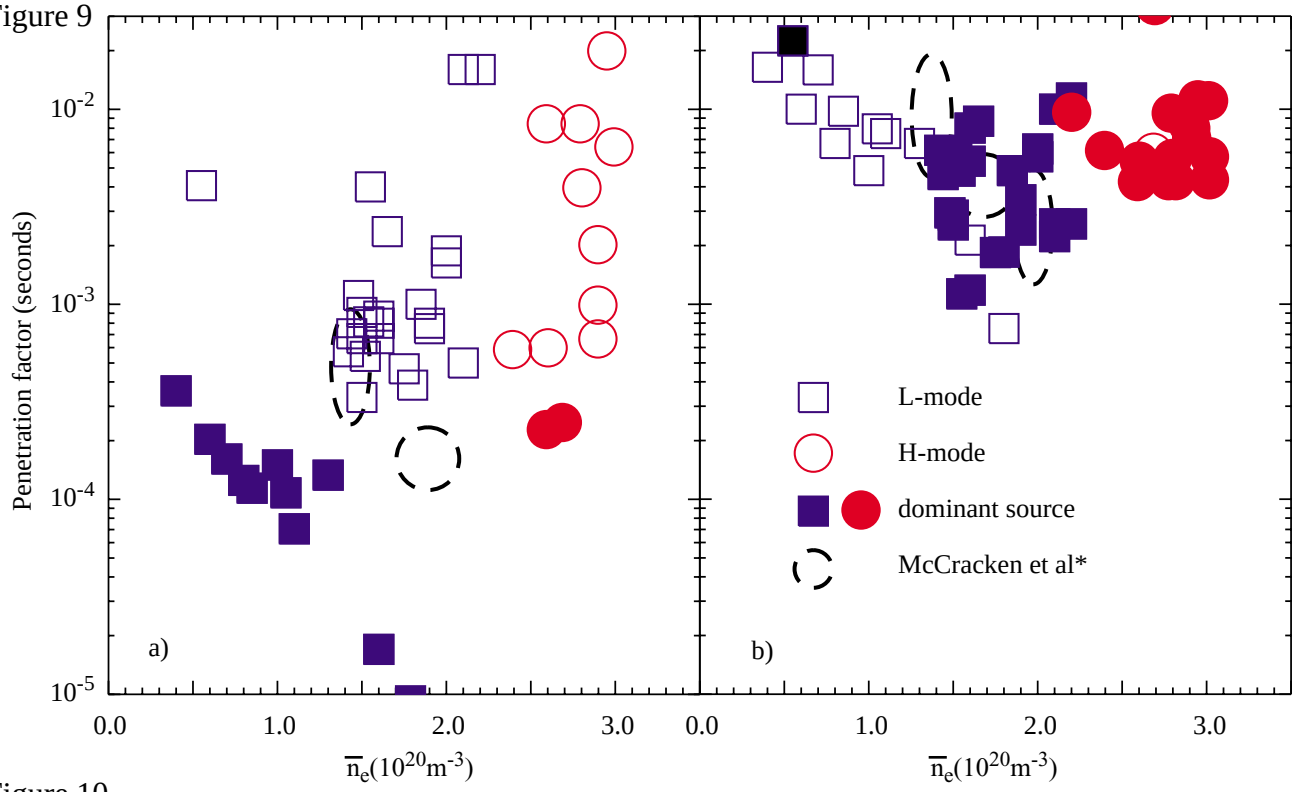

Figure 10

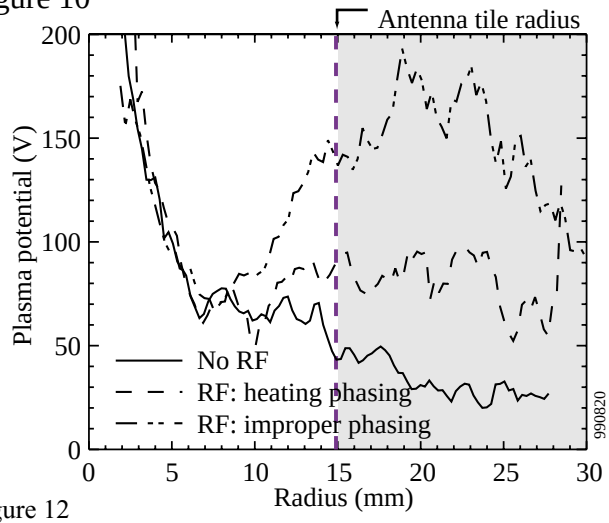

Figure 11

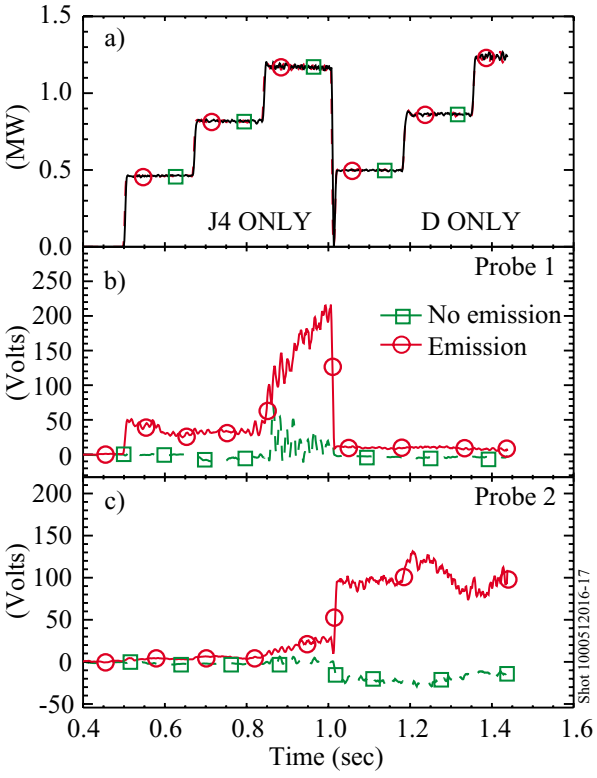

Figure 12